Development, Optimization, and In Vitro Evaluation of Folic Acid-Decorated Methotrexate/EDTA Solid Lipid Nanoparticles for Breast Cancer

[a]Meena Devi, [b]Ritu Kataria, [c]Rahul Pratap Singh, [a]Vikas Jhawat*

[a]Department of Pharmaceutical Science, School of Healthcare and Allied Science, GD Goenka University, Gurugram, Haryana, India

[b]GVM College of Pharmacy, Sonepat, Haryana, India

[c]Department of Pharmaceutics, Amity Institute of Pharmacy, Amity University, Noida, Uttar Pradesh-201313, India

Corresponding Author

Dr. Vikas Jhawat

Associate Professor

Department of Pharmaceutical Science,

School of Medical and Allied Science,

GD Goenka University,

Gurugram, Haryana, India

Jhawat231287@gmail.com

Abstract

Background: Globally, breast cancer remains the leading malignancy diagnosed among women. The rising incidence of this disease has driven the development of sophisticated nanomedicine strategies designed to surpass the therapeutic constraints of traditional interventions. For instance, standard Methotrexate monotherapy typically delivered via oral or parenteral routes frequently suffers from adverse side effect and poor therapeutic output in breast cancer treatment. To overcome the therapeutic constraints of monotherapies, combining innovative treatments can boost therapeutic performance while minimizing adverse side effects. Because cancer cell proliferation is highly reliant on essential metal ions, the metal chelator ethylenediaminetetraacetic acid (EDTA) can suppress tumor growth by effectively sequestering these micronutrients. Consequently, co-administering EDTA alongside Methotrexate (MTX) has demonstrated a pronounced inhibitory effect on breast cancer cell proliferation.

Objective: The objective of this study is to evaluate the anticancer potential of a novel co-delivery system pairing ethylenediaminetetraacetic acid (EDTA) with Methotrexate. These dual agents were integrated within solid lipid nanoparticles (SLNs) that actively targeted by using folic acid (FA) ligands to achieve maximize therapeutic outcomes and mitigate off target toxicity,

Method: To fabricate solid lipid nanoparticles (SLNs), a high-speed homogenization and ultrasonication approach was employed. The formulation was optimized using a box-behnken design (BBD) to evaluate the impact of critical variables, specifically glyceryl monostearate, poloxamer 188, and tween 80. Subsequently, folic acid was covalently attached to the nanoparticles via carbodiimide-mediated chemistry. The physicochemical attributes of the developed nanoparticles were systematically evaluated, including their particle size, polydispersity index (PDI), zeta potential, encapsulation efficiency, drug loading, and *in vitro* release profiles.

Results

The optimized SLN formulation (MTX-SLNs) demonstrated a mean particle diameter of 122.8 ± 0.37 nm, a surface charge (zeta potential) of −17.5 ± 0.57 mV, and a narrow size distribution, indicated by a polydispersity index (PDI) of 0.288 ± 0.015. This formulation achieved a high entrapment efficiency of 86.28 ± 0.37%. In comparison, the EDTA-modified counterparts (MTX-EDTA-SLNs) displayed slightly altered characteristics, with an average particle size of 123.5 ± 0.42 nm, a zeta potential of −21.2 ± 0.35 mV, and a comparable entrapment efficiency of 85.45 ± 0.56%. The drug loading efficiency was determined to be 6.75 ± 0.18% for EDTA containing SLNs and 10.17 ± 0.15% for MTX containing SLNs. The final formulation exhibited a prolonged and sustained drug release profile over 24 hours, alongside a favorable nanoparticle recovery yield of 88.93 ± 0.41%. Furthermore, hemocompatibility studies verified the safe, non hemolytic nature of the SLNs which retained their stability for up to 3 months when stored at 4 ^{O}C. *In vitro* dissolution studies verified a 24 hour sustained release pattern that fit the Korsmeyer–Peppas mathematical model for both lipid variants.

Conclusion: The precise targeting and minimized off-target impacts are driven by the coadjuvant action of EDTA, which disrupts the malignant cell membrane to facilitate enhanced therapeutic action. The findings indicate that folic acid functionalized SLNs provide a promising method for enhancing the delivery of both methotrexate with coadjuvant

EDTA that could significantly improve breast cancer treatment outcomes. The promising result from current study could support further investigation of this solid lipid nanoparticles formulation for potential clinical use in breast cancer treatment.

Keywords: Breast cancer, ethylenediaminetetraacetic acid, box behnken design (BBD)

How to cite this article: Devi M, Kataria R, Singh RP, Jhawat V. Development, optimization, and in vitro evaluation of folic acid-decorated methotrexate/EDTA solid lipid nanoparticles for breast cancer. Int J Drug Deliv Technol. 2026;16(75s): 357-377. DOI: 10.25258/ijddt.16.75s.40

1. Introduction

As a critical global health issue, breast cancer accounts for 30% of female cancer cases and results in over 500,000 annual fatalities [Saeg et al., 2018]. Even with significant breakthroughs in research and therapy, this disease continues to rank as the second deadliest cancer for women in the United States [Priyadarsini & Lahoti, 2022]. Current breast cancer treatments primarily rely on surgical intervention, radiotherapy, chemotherapy, and targeted therapies. While effective, conventional approaches like chemo and radiation frequently cause significant toxicity in healthy tissues [Chaudhari et al., 2024]. Consequently, recent oncology research has increasingly focused on discovering and developing novel therapeutic agents to improve efficacy and minimize these adverse systemic effects and the emergence of drug resistance [Niazvand, F., et al., 2019]. Overcoming acquired resistance to therapy remains one of the most critical challenges in successfully treating breast cancer [Alghnnami et al., 2025]. To bypass these therapeutic hurdles, advanced strategies particularly nanocarrier mediated targeted drug delivery and cell-specific therapeutics offer a promising avenue for enhancing breast cancer treatment efficacy [Chaudhari et al., 2024]. Methotrexate (MTX), a folic acid antagonist also known as (N-[4-[[(2, 4-Diamino-6-pteridinyl) methyl] nmethylamino] benzoyl]-L-glutamic acid or 4-Amino-N10-methylpteroyl-L-glutamic acid) serves as a foundational therapeutic agent in managing various malignancies, including carcinomas of the breast and lung, head and neck epidermoid tumors, non-Hodgkin's lymphomas, and advanced mycosis fungoides. It acts as a triple enzyme inhibitor, downregulating the activity of dihydrofolate reductase, thymidylate synthase, and 5-aminoimidazole carboxamide ribotide transformylase to halt cellular replication [Yoon et al., 2010; Mukhtar et al., 2023].

Cellular generation of vital metabolites specifically the amino acids serine and methionine, along with purines and thymidylate depends directly on the activity of these enzymatic targets. Despite demonstrating a superior safety profile over other conventional anti-cancer therapeutics, it is not entirely devoid of debilitating side effects [Khan et al., 2012; Kaplan & Pazarci, 2024]. Folate receptors on the cell surface actively transport Methotrexate into the intracellular environment. The clinical effectiveness of drug is largely limited by a resistance mechanism that impairs its active uptake via the cell receptor. Furthermore, the drug exhibits poor passive permeability across cellular membranes [Surve et al., 2021]. This research examines a novel formulation approach, co-administering MTX with EDTA to overcome transport limitations and maximize antineoplastic effect of MTX [Feril et al., 2017]. Due to its ability to form stable chemical complexes with metal ions, EDTA serves as a highly adaptable chelating agent. By effectively sequestering divalent cations (eg. Zn^{2+}, Cu^{2+}, Mn^{2+}, Fe^{2+}, Ca^{2+}) it plays a critical role in diverse fields including medicine, industrial manufacturing, and food preservation. Owing to its favorable safety profile and exceptional stability, disodium EDTA is widely utilized as the primary stabilizing and preserving agent in both pharmaceuticals and commercial food products. Divalent cations including Zn^{2+}, Cu^{2+}, Mn^{2+}, Fe^{2+}, Ca^{2+}, Mg^{2+} serve as critical regulators of the key biochemical pathways required for both normal physiological homeostasis and the proliferation of malignant cells. These ions play a vital role in signal transduction, maintain cellular structural integrity, modulate ion channel activity, and serve as essential enzymatic cofactors. Furthermore, they actively participate in various biological processes within the nucleus [Gaur, K., et al., 2018]. Within cellular environments, the metal ions maintain measurable concentrations and specifically target DNA and RNA for binding. By sequestering and elimination of vital intracellular metal ions within malignant cells, chelating agents disrupt the pivotal metabolic pathways required for tumor growth, proliferation, and metastatic progression and ultimately help in inducing lysis in malignant cells. Chelating agent also act through diverse mechanisms that ultimately arrest tumor growth, including the induction of DNA damage, perturbation of osmotic equilibrium, metabolic disruption, and altered biocatalysis. Consequently, targeting these metal ions represents a highly effective therapeutic strategy against breast cancer that may circumvent the development of drug resistance. By incorporating a chelating agent can augment the therapeutic efficacy of MTX by compromising either the structural integrity or the metabolic networks of malignant cells [El-

Naggar & El-Said, 2020]. Concomitant administration of the chelating agent EDTA has been shown to potentiate the therapeutic index of conventional chemotherapeutic agents, serving as an effective adjuvant in oncological treatments. Experimental evidence confirms that EDTA potentiates antitumor activity of cisplatin against murine colon cancer models *in vivo*. Furthermore, *in vitro* evaluations revealed notable inhibitory effects against the human breast adenocarcinoma cell line (MCF-7) [Feril et al., 2017]. Furthermore, literature indicates that the inclusion of EDTA optimizes the therapeutic performance of cisplatin when administered via localized intratumoral injection [Pajak et al., 2007]. While EDTA encapsulated in liposomes failed to exhibit independent anticancer properties, its co-encapsulation with doxorubicin successfully minimized the toxicity of drug without compromising its therapeutic efficacy [Song et al., 2014]. Across multiple in vitro studies on breast cancer, melanoma, and colon cancer cell lines, EDTA consistently demonstrated the capability of potentiating the anticancer ability of chemotherapeutic agents when used in combination (e.g., with cisplatin or doxorubicin) but it lacks significant anticancer activity as a standalone agent, especially when delivered alone in liposomal form [Kontoghiorghes, 2020]. Compared to traditional systemic drug delivery system, employing specialized nanodrug delivery vehicles for site-specific targeting in breast cancer cells provides a more potent and effective therapeutic approach [Mandadi & Srinivas, 2022]. Advanced delivery systems like nanocapsules, macromolecular conjugates, and lipid vesicles are actively engineered to bypass the limitations of standard chemotherapy and enhance targeted tumor control [Uzakova et al., 2025]. The present work successfully developed solid lipid nanoparticles (SLNs), which have attracted significant attention among contemporary colloidal drug delivery systems. Solid lipid nanoparticles (SLNs) offer distinct advantages over other nanocarriers, notably through their capacity to encapsulate both hydrophilic and hydrophobic compounds while providing sustained release kinetics and protection against enzymatic breakdown [Gidwani & Vyas, 2016]. Furthermore, these physically stable systems enhance drug solubility and bioavailability, facilitate site-specific targeting, and remain highly cost-effective [Ghasemiyeh & Mohammadi-Samani, 2018]. Furthermore, SLNs mitigate the risk of drug resistance and improve patient compliance by facilitating lowered dosing amounts and less frequent administration schedules [Mäder, 2020; Thakur et al., 2026]. SLNs are formulated from biocompatible lipids that exhibit exceptional biodegradability and minimal toxicity. Solid lipid nanoparticles are require no organic solvents for synthesis, safeguard drug integrity and possess a superior loading capacity [Mohamed, 2025]. Furthermore, solid lipid nanoparticles can augment membrane structural integrity while simultaneously mitigating the premature drug-leaching issues typically associated with traditional formulations [Bhagwat et al., 2020].These characteristics make SLNs attractive potential carriers for improving the delivery of drugs with unfavorable physicochemical properties. To enhance their specificity for malignant tissues, SLNs can be surface-functionalized with various targeting ligands, including biotin, transferrin, HER2, or folic acid (FA). Based on this approach, the current study employs folic acid to actively target folate receptors, which are characteristically overexpressed on the surface of breast cancer cells [De et al., 2023]. Due to the intrinsic affinity between folic acid and its corresponding receptors on tumor cells, this strategy provides a highly efficient mechanism for targeted drug delivery. Consequently, this approach helps mitigate the severe adverse effects associated with systemic free drugs and aids in overcoming multidrug resistance [Gunduz et al., 2014]. To achieve optimal SLN performance, researchers should refine processing parameters and adjust nanoparticles characteristics like morphology, mean diameter, and drug release kinetics [Das et al., 2011; Zhang et al., 2010]. To establish the optimal parameters for fabricating solid lipid nanoparticles with targeted properties, the study integrated a box-behnken design (BBD) alongside response surface methodology [Cassayre et al., 2025]. This mathematical framework enables a precise evaluation of the interactions between designated independent variables and their corresponding outputs. Specifically, the formulation parameters were evaluated using a three-factor, three-level BBD configuration executed with three replicates. The objective of this study is to evaluate the in vitro synergistic anticancer efficacy of folic acid decorated solid lipid nanoparticles (SLNs) co-loaded with Methotrexate (MTX) and EDTA (chelating agent) against breast cancer cells.

2. Materials and methods

2.1 Materials

Methotrexate (MTX) was generously provided as a gift sample by Zenotech Laboratories Limited (Hyderabad, India). Spruce Enterprises (Ambala Cantt, Haryana, India) was the source for Poloxamer 68, Tween 80, and glyceryl monostearate, EDC, NHS. For purification and release studies, a dialysis membrane featuring a 2.4 nm pore size and a molecular weight cut-off (MWCO) of 12,000–14,000 Da was obtained from Hi-Media (Mumbai, India). All additional chemicals and reagents utilized throughout

this research were of analytical grade and utilized without further purification.

2.2 Preparation of solid lipid nanoparticles

Methotrexate (MTX)-loaded solid lipid nanoparticles (SLNs) were fabricated via a modified high-shear homogenization and probe-sonication technique, utilizing glyceryl monostearate as the solid lipid matrix alongside poloxamer 68 and tween 80 as the surfactant and co-surfactant, respectively. The specific quantity of the lipid was melted in a beaker by raising the temperature to 70 °C. 6 mg of the chemotherapeutic agent (MTX), was uniformly dispersed within the molten lipid phase. Concurrently, an aqueous phase was prepared in a separate vessel by dissolving the designated amounts of surfactant and co-surfactant in 10 mL of distilled water, which was pre-heated to an identical temperature of 70 °C. Under continuous, vigorous magnetic stirring at 850 rpm on a hot plate, the heated aqueous phase was introduced dropwise into the lipid melt. The resulting pre-emulsion was immediately subjected to high-speed homogenization at 10,000 rpm for 10 min. To counteract heat generation during this intense shearing process, the container was kept immersed in an ice bath. Finally, the system was probe-sonicated for an additional 5 min to achieve the desired nanoparticle dimensions [Elsayed & Belal., 2021].

2.2. Preparation of Methotrexate/ EDTA solid lipid nanoparticles

EDTA/ Methotrexate solid lipid nanoparticles (SLNs) were synthesized using a slightly modified procedure. The aqueous phase was initially prepared by dissolving the surfactants in 10 mL of distilled water, followed by the addition of a designated quantity of EDTA. To continue the process, the aqueous phase was brought to 65-70°C while a specific mass of glyceryl monostearate was melted separately at 65°C. Methotrexate was then added directly into the molten GMS. Keeping the temperature stable to avoid crystallization, the heated lipid phase was slowly combined with the hot aqueous phase under high-shear homogenization. Homogenization of the mixture was carried out at 10,000 rpm for a duration of 10 minutes. The resulting oil-in-water (O/W) emulsion was subsequently treated with probe ultrasonication for 5 minutes, a critical step utilized to diminish the particle size down to the nanometer scale. The carboxyl groups of EDTA facilitate binding to the lipid surface. Subsequently, the emulsion was rapidly cooled to 4°C, inducing the solidification of the lipid matrix and successfully encapsulating the drugs within the solid lipid nanoparticles [Sreeharsha et al., 2025].

2.2.2 Optimization via Box Behnken Design

To optimize the formulation, a 17run Box-Behnken design featuring three factors across three distinct levels was utilized. The independent variables evaluated were glyceryl monostearate (X1), Smix (1:3 ratio of poloxamer 68 to tween 80) (X2), and sonication time (X3). Conversely, particle size (Y1), zeta potential (Y2), and the percentage of entrapment efficiency (Y3) were designated as the dependent responses. All three independent factors demonstrated a significant impact on the particle size (Y1), zeta potential (Y2), and entrapment efficiency (Y3). In this design, variables were assigned three levels: high (+1), medium (0), and low (−1). A total of 17 experimental runs were carried out as detailed in Table 1. To ensure accuracy, all trials were executed in triplicate, and results are reported as mean ± SD. Equation 1 details the quadratic model generated for these variables to identify the optimum region

$$Y=\alpha_o+ \alpha_1 X_1+ \alpha_2 X_2+ \alpha_3 X_3+ \alpha_{12} X_1 X_2+ \alpha_{13} X_1 X_3+ \alpha_{23} X_2 X_3+ \alpha_{11}X_1^2 + \alpha_{22}X_2^2 + \alpha_{33}X_3^2 \quad (1)$$

In this model, Y represents the dependent response variable, α_o signifies the intercept, and $\alpha_1, \alpha_2, \alpha_3$ denote the linear regression coefficients for the independent factors X1, X2, and X3. Furthermore, the interaction terms are represented by α_{12}, α_{13}, and α_{23} while α_{11}, α_{22}, and α_{33} designate the quadratic coefficients. The statistical significance of the model for each individual response was evaluated using analysis of variance (ANOVA). To visualize how the variables influenced these responses, three-dimensional (3D) response surface plots were generated. All design of experiments (DoE) statistical computations were executed using Design-Expert software (Trial version 12.0.0, Stat-Ease, Inc., MN, USA). [Lalchandani et al., 2024].

Table 1: Outlines the independent factors and their respective levels designated as low (-1), medium (0), and high (+1) used during the statistical optimization of the SLNs.

	Levels employed		
Independent variables (factors)	**Low (-1)**	**Medium (0)**	**High (+1)**
X1: Glyceryl monostearate (mg)	100	200	300
X2: Smix (mg) (Poloxamer 188: tween 80)	300	400	500
X3: Stirring speed (rpm)	1	3	5
Dependent variables (responses)	**Constrains**		
Y1:Particle size (nm)	Minimize		
Y2: Zeta potential (mV)	In range		

Drug loading (%) = [Amount of drug in SLNs] × 100

Y3: Entrapment efficiency (%)	Maximize

Table 2: The independent factors selected in the experimental design to establish the experimental runs

Experimental Run	GMS (%w/v) X1	(Poloxamer: Tween 80) (mg) X2	Sonication time (min) X3
1	100	500	3
2	100	400	5
3	200	500	5
4	200	400	3
5	200	400	3
6	200	500	3
7	300	300	1
8	200	400	5
9	300	300	3
10	300	400	1
11	100	400	3
12	200	300	5
13	200	400	3
14	200	500	1
15	100	300	3
16	300	400	1
17	200	400	3

Drug loading (%) = [Amount of drug in SLNs] × 100

3. Characterization

3.1 Measurement of mean particle size, PDI and zeta potential

To evaluate the physical characteristics of the prepared SLNs, dynamic light scattering (DLS) was performed using a Malvern Zetasizer Nano ZS 90 at a fixed temperature of 25°C and a 90° scattering angle. This analysis provided both the mean particle diameter (z-average) and the polydispersity index (PDI) to quantify the breadth of the size distribution. To minimize opalescence, the SLN samples were first diluted using double-distilled water. The same Zetasizer equipment was then operated at 25°C to determine the zeta potential, tracking the surface charge in millivolts (mV). All experimental data were gathered from three independent measurements [Surve et al., 2021; Gidwani & Vyas, 2016].

3.2 Transmission Electron Microscopy (TEM)

To evaluate the nanostructure of nanoformulation such as MTX-SLNs and MTX-EDTA-SLNs, transmission electron microscopy (TEM) was performed. Briefly, a single drop of the nanoformulation was deposited onto a film-coated copper grid. The sample laden grid was subsequently stained by applying a 1% (w/v) phosphotungstic acid solution to its surface. After allowing the grid to air-dry, microscopic images were captured using a TEM instrument (JEM-1010; Jeol Ltd., Tokyo, Japan) [Suvarsha, 2020; da Rocha et al., 2020].

3.3 Determination of % entrapment efficacy, % NPs yield and drug loading (%)

To evaluate the quantity of free drug, the prepared MTX-SLNs were spun down in a centrifuge at 7,000 rpm for 45 minutes. The clear supernatant was then harvested and analyzed using UV spectrophotometry to quantify the unentrapped methotrexate. A calibration curve, established from known concentrations of drug solutions, was employed to calculate the exact amount of unloaded drug. Finally, entrapment efficiency (EE%), NPs yield (%), and drug loading capacity (%) were calculated according to the equations detailed below. [Gidwani & Vyas., 2016; Dadashi, H., et al., 2024].

$$\% \text{ Entrapment efficiency} = \frac{[\text{Total amount of drug} - \text{free amount of drug}]}{\text{Total amount of the}} \times 100$$

$$(\%) \text{ NPs yield} = \frac{[\text{Weight of the nanoparticles}]}{\text{Total weight of drug + polymer}} \times 100$$

3.4 Determination of the drug loading (%) of EDTA in solid lipid nanoparticles

To measure EDTA drug loading (%), the SLN dispersion was centrifuged at 7,000 rpm for 45 minutes. The resulting supernatant was isolated and analyzed via UV-Vis spectrophotometry against a standard curve of known drug concentrations to determine free EDTA content and subsequent loading efficiency as

3.5 Transmission electronic microscopy (TEM)

We evaluated the surface morphology and structure of the MTX-SLNs using a transmission electron microscope (TEM; JEM-1400Plus, JEOL Co., Japan) set at 200 kV. Sample preparation involved diluting the freshly prepared MTX-SLN dispersion 10-fold in aqueous solution, dropping it onto a carbon-grid copper mesh, and drying it under ambient room conditions before TEM analysis [Surve et al., 2021].

3.6 Optimization of SLNs nanoparticles

The preliminary optimization experiments to screen the key process and formulation factors controlling SLN fabrication. The results demonstrated that mixing speed, sonication period, and the concentrations of lipid and surfactant markedly influenced nanoparticle size, zeta potential, and drug loading efficiency. A Box–Behnken response surface methodology was applied to optimize three key parameters: sonication duration (min), lipid ratio, and surfactant content, all of which markedly influenced particle size, zeta potential, and entrapment percentage. Analysis of variance (ANOVA) modeling was subsequently utilized to identify the ideal operational values for these independent factors.

3.7 EDTA modified optimized solid lipid nanoparticles

The optimized MTX-SLNs were further modified by incorporating EDTA. A measured quantity of EDTA was dissolved into the aqueous phase while stirring continuously. This aqueous mixture was then added dropwise into the oil phase, which contained methotrexate (MTX) and glyceryl monostearate, and the combined system was stirred for 30 minutes. The mixture was emulsified using a high-speed homogenizer at 10,000 rpm for 10 minutes, then sonicated for 5 minutes. The resulting MTX-EDTA-SLNs were subsequently characterized for particle size, zeta potential (surface charge), and morphology.

3.8 Folic acid decorated EDTA modified optimized solid lipid nanoparticles

The MTX-EDTA-SLNs were linked to folic acid (FA) using carbodiimide chemistry. FA was activated through its carboxyl group in the presence of NHS and EDC before covalent coupling. Specifically, 7 mg of FA dissolved in 14 mL of phosphate buffer (0.01 M, pH 7.4) was activated with 14 mg EDC and 7 mg NHS while stirring at 100 rpm and 25°C for 1 hour. The activated FA solution was mixed with the MTX-EDTA-SLNs and the reaction mixture was left at room temperature for 2 hours to produce FA-MTX-EDTA-SLNs. The FA-conjugated SLNs were then dialyzed against PBS using a 12 kDa cut-off dialysis bag for 60 minutes to remove unreacted ligand and other impurities. [Yassemi et al., 2020].

3.9 *In vitro* drug release and kinetic studies

The dialysis bag method was employed to assess drug release from optimized MTX-SLNs, MTX-EDTA-SLNs, and free MTX in two media: pH 7.4 (physiological) and pH 5.5 (tumor-like acidic environment). Prior to use, dialysis membranes (MWCO 12,000–14,000 Da, pore size 2.4 nm) were soaked overnight in PBS pH 7.4. Each release study used 30 mL of the respective release medium (pH 7.4 or pH 5.5). For the release experiments, 1 mL of the SLN suspension (containing 600 µg MTX) was placed into a dialysis bag. The release was carried out at 37 ± 0.5 °C with continuous stirring at 100 rpm. At 0.5, 1, 2, 4, 6, 8, 12, and 24 hours, 1 mL samples were withdrawn from the release medium and immediately replaced with 1 mL of fresh PBS (pH 7.4 or pH 5.5) to keep the volume constant. MTX levels were quantified by UV visible spectrophotometry at 258 nm. All measurements were performed in triplicate. The cumulative percentage of drug released was calculated and plotted versus time. Release data were fitted to several kinetic models zero-order, first-order, Higuchi, Korsmeyer–Peppas, and Hixson–Crowell to determine the drug release mechanism. The model that best described the release was selected based on the highest regression coefficient (R2). All experiments were performed in triplicate [Priyadarsini & Lahoti, 2022; Kakkar et al., 2015].

3.11 Hemolysis study

Hemocompatibility of free MTX, optimized MTX-SLNs, and MTX-EDTA-SLNs was determined through red blood cell membrane integrity assays. Freshly drawn blood (20 mL) obtained from a rotary club in Gurugram, India, was centrifuged at 2,000 rpm for 10 minutes at 25 °C. We removed the supernatant, washed the isolated erythrocytes three times in PBS (pH 7.4), and gently resuspended them in 50 mL saline. For controls, we designated 1% Triton X-100 as 100% lysis (positive) and normal saline as 0% lysis (negative). Aliquots (0.4 mL) of each formulation containing equivalent drug concentrations were mixed with 1.6 mL of the erythrocyte suspension and incubated at 37 °C. Over 0.5-4 hours, 2 mL samples were retrieved at set intervals and centrifuged at 2,000 rpm for 10 minutes. The released hemoglobin in the supernatant was analyzed at 540 nm using a UV–Vis spectrophotometer to calculate the percentage of hemolysis [Devi et al., 2026; Yadav et al., 2023; Dumoga et al., 2016].

$$\% \text{ Hemolysis} = B_{(\text{test sample})} - B_{(\text{negative control})} / B_{(\text{positive control})} - B_{(\text{negative control})} \times 100$$

Statistical analysis: Statistical analysis was conducted using one-way ANOVA, with data presented as mean ± SD (n = 3). Differences were deemed statistically significant at $p < 0.05$.

4. Stability studies

To evaluate the physicochemical stability of the formulations, three-month stability testing was performed under distinct thermal conditions: refrigeration such as (4°C± 1°C), room temperature (25 ± 1°C), and accelerated storage (40 ± 1°C). The samples were sealed tightly throughout the study and periodically evaluated for changes in particle size, zeta potential, and entrapment efficiency percentage [Rajpoot et al., 2018].

5. Result and Discussion

5.1 Preparation and optimization of solid lipid nanoparticles

Based on insights from preliminary optimization studies, a three-factor, three-level box-behnken Design (BBD) was utilized to assess both main and interaction effects of key process variables. Three independent parameters was evaluated such as GMS concentration (X1), Smix concentration (X2), and sonication time (X3) at low (-1), medium (0), and high (+1) levels. Their direct impact was measured on three dependent variables: particle size (Y1), zeta potential (Y2), and % entrapment efficiency (Y3). As detailed in Table 3, the independent parameters were investigated at three distinct levels (low, medium, high): GMS concentration (X1: 100, 200, 300 mg), Smix concentration (X2: 300, 400, 500 mg), and sonication duration (X3: 1, 3, 5 min). The interactive influences of these factors were visualized using three dimensional response surface plots (Figure 1). A total of 17 experimental runs were executed to systematically assess the impact of process conditions on particle size, zeta potential, and entrapment efficiency (%). The data were best fitted to a quadratic model, as confirmed by R^2 values approaching unity. The generated polynomial equations effectively captured the linear, interactive, and higher order quadratic effects of the inputs on the responses. The regression model summary statistics for particle size (Y1), zeta potential (Y2), and sonication time (Y3) are outlined in Table 4.

Table 3: The formulations and the experimental results of the optimization DoE

Experimental run	Independent Variables			Dependent Variables		
	Factor1	**Factor 2**	**Factor 3**	**Response 1**	**Response 2**	**Response 3**
	X1: GMS (mg)	**X2: Smix (1:3) (mg)**	**X3:Sonication time (min)**	**Particle size (nm) Y1**	**Zeta Potential (mV) Y2**	**EE (%) Y3**
F1	100	500	3	171.6±0.47	-18.11 ±0.23	75.76±0.33
F2	100	400	5	173.96±0.67	-18.71 ±0.21	76.67±0.89
F3	200	500	5	130.48±0.56	-20.1± 0.34	86.54±0.55
F4	200	400	3	131.41±0.89	-20.21 ±0.36	87.78±0.61
F5	200	400	3	128.6±0.52	-20.13 ±0.52	86.65±0.31
F6	200	500	3	125.6±0.62	-20.23 ±0.42	86.48±0.29
F7	300	300	1	167.9±0.35	-17.4± 0.36	75.55±0.65
F8	200	400	5	130.61±0.41	-18.6± 0.73	87.68±0.43
F9	300	300	3	178.1±0.45	-12.3± 0.28	77.67±0.41
F10	300	400	1	178.8±0.57	-12.13 ±0.34	77.33±0.31
F11	100	400	3	181.5±0.63	-16.31 ±0.67	76.61±0.45
F12	200	300	5	128.4±0.42	-18.61 ±0.32	87.23±0.23
F13	200	400	3	119.48±0.76	-20.92 ±0.12	86.42±0.33
F14	200	500	1	123.78±0.52	-18.13 ±0.43	85.46±0.51
F15	100	300	3	182.91±1.45	-16.2± 0.63	75.73±0.38
F16	300	400	1	176.51±0.78	-13.1± 0.54	77.73±0.48
F17	200	400	3	132.81±0.65	-20.24 ±0.31	85.87±0.39

X1: GMS (mg); X2: Smix (1:3) (mg); X3: Sonication

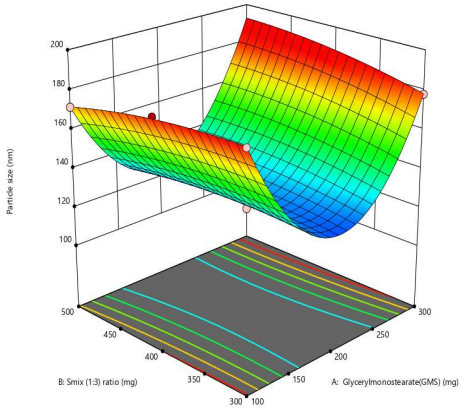

time (min); Y1: Particle size (nm); Y2: Zeta potential (mV); Y3: EE% (%) Values are in mean±SD, n=3

Table 4: Model summary statistics for regression analysis of responses Y1, Y2, and Y3

Response	Source	F-Value	p-value Prob >F	Inference	R^2	Adj. R^2	Pred. R^2	Adeq. precision
Y1 (Particle size)	Model (Quadratic)	69.34	<0.0001	Significant	0.9889	0.9746	0.9751	19.1543
	Lack of fit	0.0457	0.9852	Non-significant				
Y2 (Zeta potential)	Model (Quadratic)	112.50	<0.0001	Significant	0.9931	0.9843	0.9793	29.3572
	Lack of fit	0.0279	0.9928	Non-significant				
Y3 (Entrapment efficiency)	Model (Quadratic)	154.75	<0.0001	Significant	0.9950	0.9886	0.9805	28.1989
	Lack of fit	0.11760	0.9461	Non-significant				

5.2 Response surface methodology and contour plots analysis of optimized solid lipid nanoparticles

The contour plots and 3D response surface plots were analyzed and presented in Figure 1.

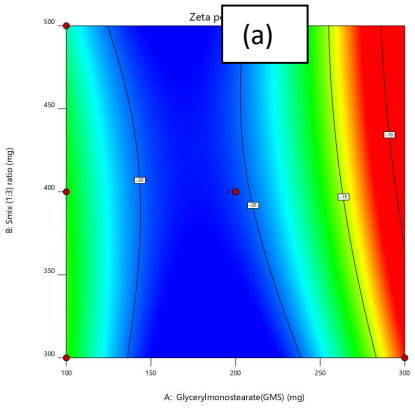

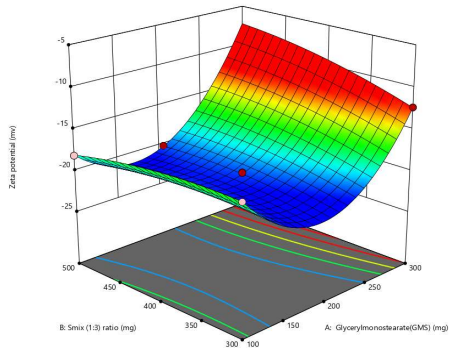

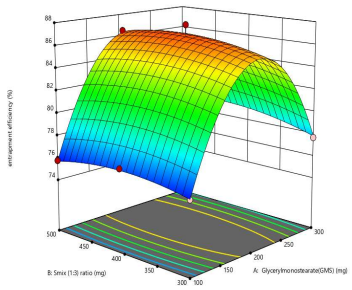

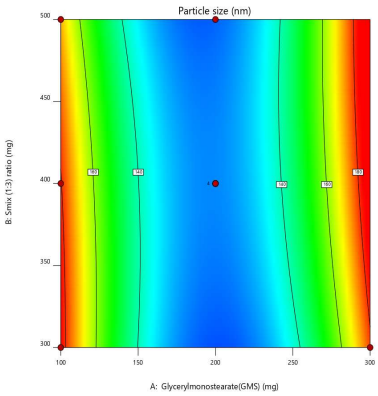

(b)

Figure 1: Two-dimensional (2D) contour diagrams and three-dimensional (3D) response surface plot for (a) particle size, (b) zeta potential, (c) % entrapment efficiency

5.3 Interaction effect of input parameters on the response parameters

Both GMS and the surfactants mix (Smix, 1:3) demonstrated a strong impact on the mean particle size of the synthesized solid lipid nanoparticles. Among all evaluated process variables including surfactant concentration and sonication duration GMS proved to be the primary determinant of nanoparticles size. Based on the box-behnken design, the relationship between these factors and mean particles size was best fitted to a quadratic model, expressed by the following polynomial equation:

$$Y1 = 128.05 + 3.97A + 0.6387B + 2.37C + 6.47AB + 9.94AC + 0.5395BC + 56.47A^2 - 2.98B^2 + 1.29C^2 \quad (2)$$

In above polynomial equation, a positive sign indicates a synergistic relationship, where the variables interact positively to have a greater combined effect. On the other hand, a negative sign indicates an antagonistic relationship, where variables interact negatively, resulting in a combined effect that is less than the sum of individual effects. Factor A (Glyceryl monostearate), B (Smix) and C (sonication time) exerted a positive influence on particle size (Y1). The interactive terms AB, AC, and BC showed positive impact on particle. Box-behnken design analysis established quadratic polynomial equations for zeta potential (Y2) and % entrapment efficiency (Y3) as follows.

$$Y2 = -20.36 + 3.66A + 0.8050B + 0.5891C + 1.74AB + 4.11AC - 1.55BC + 7.64A^2 - 0.7303B^2 + 1.16C^2 \quad (3)$$

$$Y3 = 86.72 + 1.39A + 0.3252B + 1.06C + 0.3601AB + 0.5136AC - 0.5634BC - 8.86A^2 - 0.7381B^2 - 0.1946C^2 \quad (4)$$

Statistical evaluation revealed that factors A, B and C exerted a positive effect on response zeta potential (Y2) as well as entrapment efficiency percentage (Y3). Furthermore, interaction pairs AB and AC promoted higher entrapment efficiency (Y3), whereas the BC interaction exhibited a negative influence. Across the 17 experimental runs, the mean particle dimensions varied between 119.48±0.76 nm to 182.91±1.45. The concentrations of both GMS and the surfactants system markedly governed the average particle size of the solid lipid nanoparticles. To illustrate, batch F1 formulated using 100 GMS yielded a particle size of 171.6±0.47 nm, whereas batch F10 containing 300mg GMS displayed an increased diameter of 178.8±0.57 nm. At a moderate GMS level of 200mg, formulation F17 exhibited a mean particle size of 132.81±0.65 nm. Alterations in the surfactant mixture (Smix) concentration similarly exerted a substantial influence on the dimensions of the solid lipid nanoparticles. Specifically, F5 (300 mg, Smix1:3) produced particles of 182.91±1.45 nm, whereas F11 (400 mg) and F14

(500 mg) recorded smaller values of 181±0.63nm and 123.75±0.52 nm, respectively. Sonication duration also played a key role in modulating particle dimensions: extending the sonication period from 1 min (F7, 167.9± 0.35) to 3min (F5) reduced the size to 128.6± 0.52 nm. The 3D response surface graphs in Figure 1 illustrate the interactive effects of these independent variables on mean nanoparticle size. Furthermore, ANOVA statistical evaluation (Table 4) verified a significant relationship ($p < 0.05$) between the average particle diameter (Y1) and parameters A, B, and C. Furthermore, the model's R^2 goodness-of-fit statistic demonstrated that 99.89% of the variance in mean particle diameter was explained by the regression equation. Relative influence among the three formulation factors followed the sequence: GMS concentration>surfactants concentration >sonication time. Additionally, zeta potential measurements for the formulated nanoparticles batches were bounded between -12.3 mV and -20.92 mV.The presence of GMS in the solid lipid nanoparticle formulation confers a negative surface charge onto the particles. Across all 17 solid lipid nanoparticle batches (F1–F17), an elevation in GMS concentration consistently led to more negative zeta potential values. Owing to its non-ionic nature, the surfactant mixture (Smix) exerted minimal to no significant influence on the development of a negative surface charge on the solid lipid nanoparticles. As illustrated by the 3D response surface graphs in Figure 1, the formulation parameters such as GMS level, surfactant (Smix) concentration, and sonication duration exerted distinct impacts on both zeta potential and entrapment efficiency percentage. Regarding their effect on the surface charge of the solid lipid nanoparticles, the independent variables ranked in the following order: surfactant (Smix) content > GMS amount > sonication time.

As detailed in Table 4, the correlation between zeta potential (Y2) and input factors A, B, and C was statistically confirmed at a 95% confidence interval ($p < 0.05$). Additionally, R^2 fit statistics indicated the model captured 99.31% of zeta potential variation. Similarly, ANOVA analysis verified a significant influence of independent variables A, B, and C on percent entrapment efficiency (Y3, $p < 0.05$). Among these factors, GMS mass was the primary determinant of entrapment efficiency (%EE), followed by sonication time and surfactant (Smix) concentration. The fitted model for %EE displayed an R^2 value of 99.50%, reflecting excellent alignment with the experimental data.

5.4 Analysis of optimum solid lipid nanoparticles

To determine the ideal solid lipid nanoparticles (SLN) formulation, numerical optimization was employed to minimize particle size, achieve a stable zeta potential, and maximize entrapment efficiency (%EE). Experimental validation closely matched the predicted parameters of model, yielding a desirability score near to 1.0, which demonstrates the high robustness and reliability of the optimized system. The optimized methotrexate-loaded solid lipid nanoparticles (MTX-SLNs) were formulated using 200 mg of glyceryl monstearate (GMS), 300 mg of surfactant mixture (Smix), and a 5-minute sonication duration. A comparison between the predicted model values and empirical data showed small variations in mean particle size (127.5 nm vs. 122.8± 0.42 nm), zeta potential (-18.58 mV vs. -17.5 ± 0.57 mV), and %EE (87.09% vs. 86.28 ± 0.37 %). Although a statistically significant difference ($p < 0.05$) was detected between theoretical estimates and lab observations, the resulting surface charge (-18.58 mV) reflects sufficient colloidal stability for the final system (Table 5)

Table 5: The predicted and experimental values for optimized solid lipid nanoparticles

Optimized formula	GMS (X1) (mg)	Smix (X2) (mg)	Sonication time (X3) (rpm)	
	200	300	5	
Responses		**Software predicted value**	**Experimental determined value**	**p value**
Particle Size (Y1)(nm)		127.5 nm	122.8 ±0.42 nm	0.14
Zeta potential (Y2) (mV)		-18.58 mV	-17.5 ± 0.57 mV	0.02
Entrapment efficiency (Y3) (%)		87.09%	86.28 ± 0.37%	0.019

Software predictions for the optimized formulation indicated a mean particle diameter of 127.5 ± 0.30 nm, a zeta potential of -18.58 ± 0.62 mV, and a PDI of 0.280. The batch achieved a drug entrapment efficiency of 87.09 ± 0.98%, demonstrating a narrow, unimodal size distribution with reproducible features. The low PDI (0.280) confirms the high degree of homogeneity and monodispersity across the colloidal system. This negative surface charge (-18.58 ± 0.62 mV) is primarily driven by the ionization of carboxylate groups or free fatty acids present in the lipid core. Figure 2 depicts the particle size and surface charge distributions, whereas TEM micrographs verify distinct, well-dispersed, sub-micron particles with consistent and stable morphology.

6.
Characterization

6.1 Particle size, zeta potential, and TEM study of optimized solid lipid nanoparticles

The optimized MTX-SLN system demonstrated an average particles size of 122.8 ± 0.37 nm alongside a zeta potential of -17.5 ± 0.57 mV, confirming the successful preparation of physically stable solid lipid nanoparticles. Transmission electron microscopy (TEM) micrographs revealed predominantly smooth, spherical particles displaying high morphological uniformity. As illustrated in Figure 2 and detailed in Table 5, the particle sizes determined via TEM aligned closely with the dynamic light scattering (DLS) measurements.

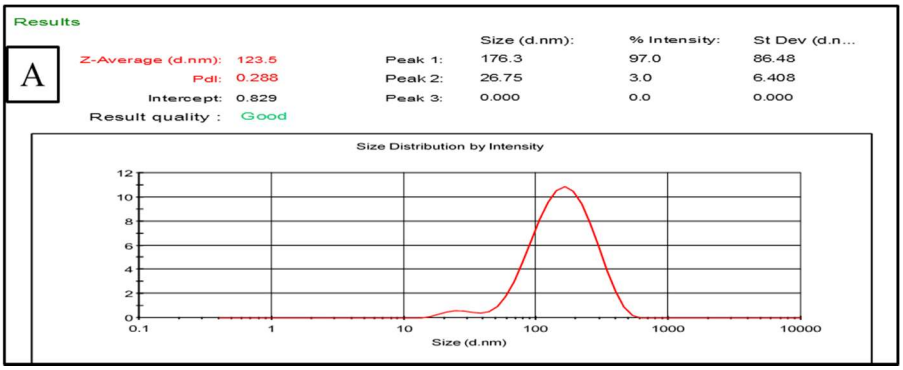

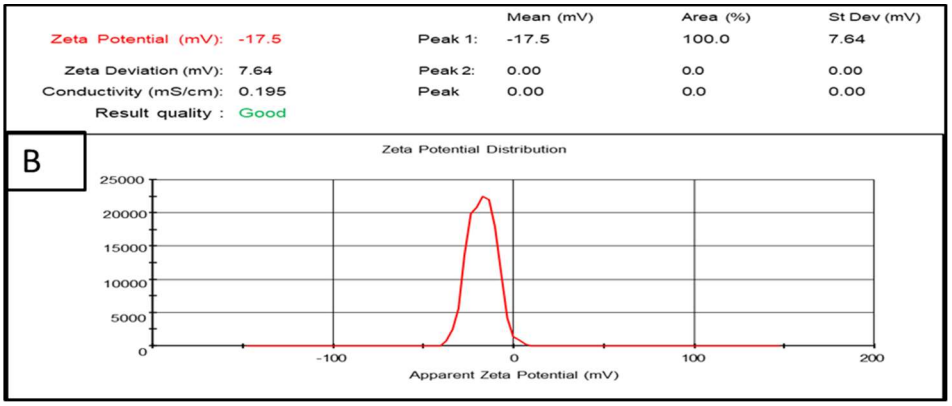

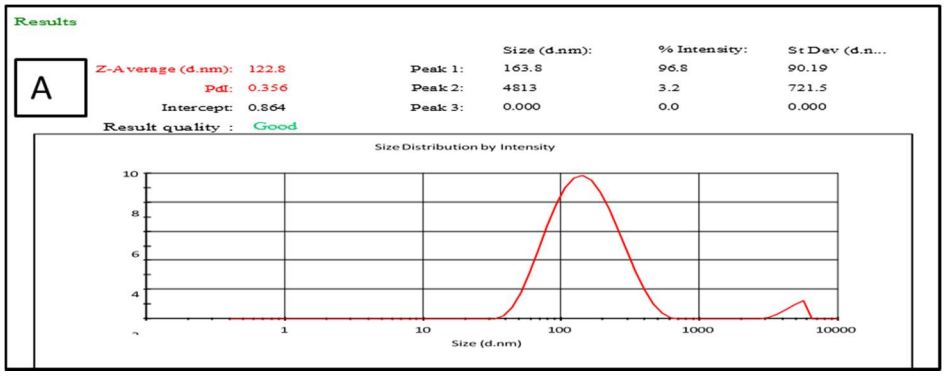

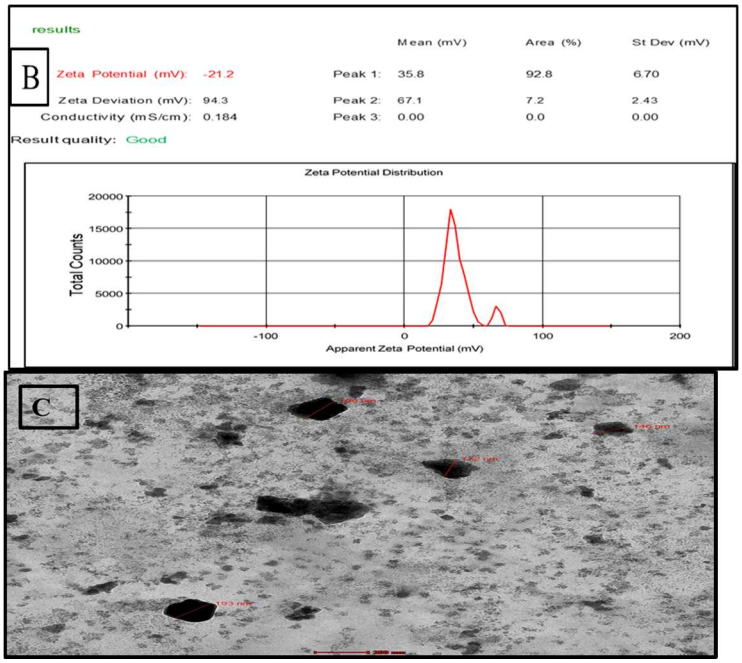

Figure 2: Representative data of independent experimental results for (A) Particle size, (B) Zeta potential, and (C) TEM image of optimized MTX -SLNs (Scale =200nm)

6.2 Particle size, zeta potential, and TEM analysis of EDTA incorporated SLNs nanoparticles

The optimized MTX-EDTA-SLNs displayed a mean particles size of 123.5 ± 0.42 nm and a surface potential of -17.5 ± 0.35 mV, confirming the successful formation of physically stable nanoparticles. Furthermore, TEM micrographs validated that the particles possessed a smooth surface texture and a highly uniform shape, as illustrated in Figure 3.

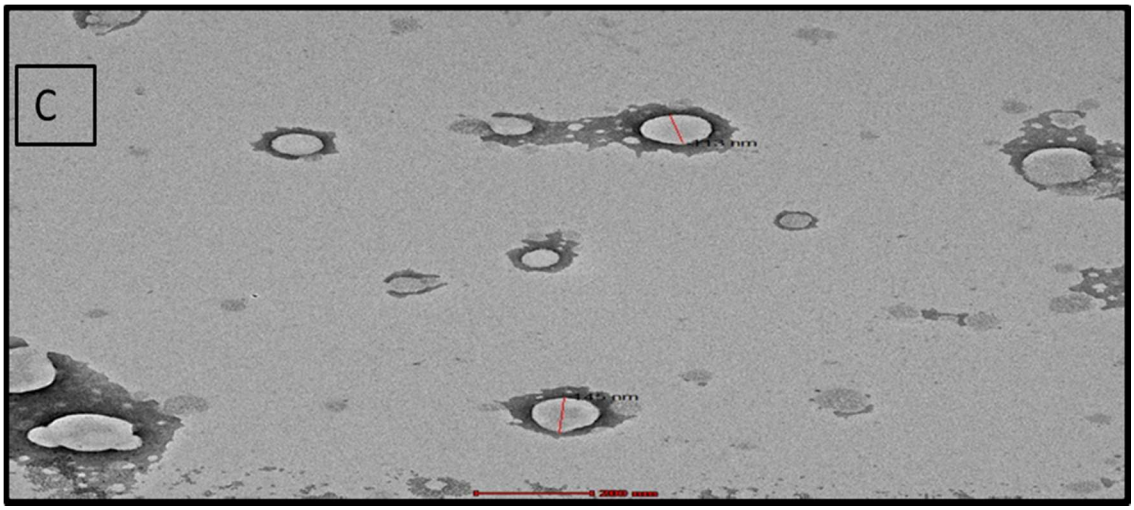

Figure 3: Representative data of independent experimental results for (A) Particle size, (B) Zeta potential, and (C) TEM image of MTX-EDTA-SLNs (Scale=200nm)

6.3 EDTA loading

UV-visible spectrophotometric analysis revealed a drug loading (DL) of 6.75 ± 0.18% for EDTA within the solid lipid matrix, demonstrating a strong, robust interaction between the lipid matrix and the chelating molecule. This loading capacity is primarily governed by the cross-linking diffusion of EDTA into the interior lipid network. Moreover, these findings highlight remarkable formulation stability, confirming that EDTA was effectively encapsulated within the nanoparticle core rather than loosely adsorbed onto the outer surface.

6.4 *In vitro* drug release study

Using the dialysis membrane approach, we evaluated the *in vitro* release behavior of free MTX alongside optimized MTX-SLNs and MTX-EDTA-SLNs at physiological pH 7.4 and endosomal/tumor-like acidic pH 5.5 (Figure 4). Under physiological conditions pH 7.4, unformulated MTX achieved rapid dissolution, releasing 94.79± 1.12% within 4 hours. Conversely, the nanoparticle formulations exhibited biphasic kinetics: MTX-SLNs and MTX-EDTA-SLNs produced an early burst effect at 1 hour (24.49± 2.25 and 33.43± 1.52), transitioning into sustained diffusion that reached 79.51±2.29 and 85.83± 2.43 by 24 hours. Similarly, at pH 5.5, plain drug release reached 95.85 ±2.17 in 4 hours, whereas MTX-SLNs and MTX-EDTA-SLNs released 29.54 ±2.15 and 37.39±1.26 at 1 hour, eventually achieving 87.51 ±2.14 and 96.83± 2.12 cumulative release over 24 hours. The early rapid release is governed by the desorption of surface-adsorbed drug, whereas the extended release over 24 hours confirms sustained entrapment within the lipid core.

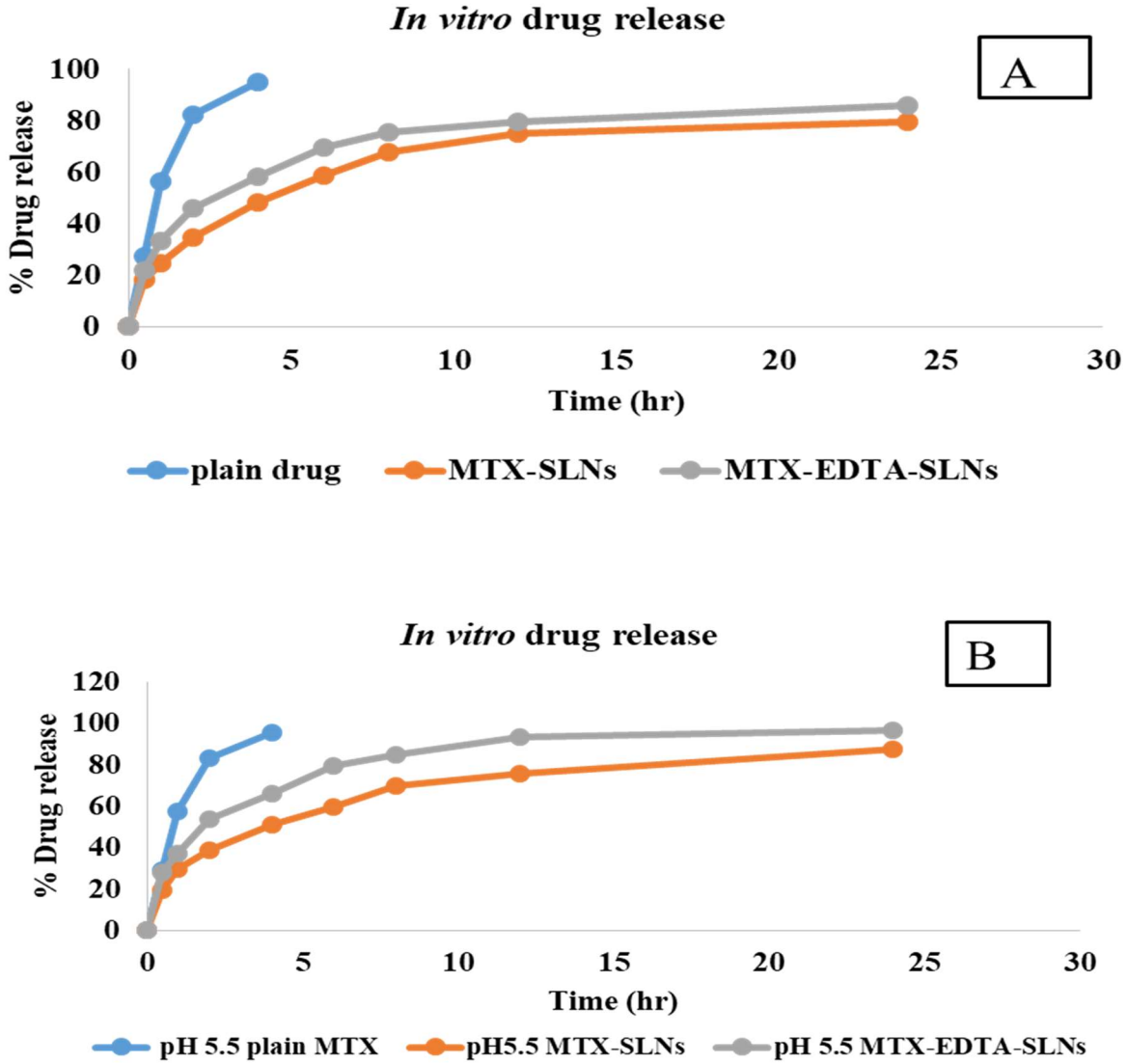

Figure 4: In vitro drug release analysis of Plain drug (MTX), MTX-SLNs, MTX-EDTA-SLNs, (A) at physiological pH 7.4 and (B) at acidic pH 5.5 (results are represented as the mean± SD for three replicates)

6.5 Evaluation of release kinetics

Mathematical modeling of in vitro release data was employed to elucidate the underlying release kinetics and determine the governing release mechanism for free MTX, MTX-SLNs, and MTX-EDTA-SLNs. The experimental release profiles were fitted to standard kinetic models, including zero-order, first-order, Higuchi, Hixson–Crowell, and Korsmeyer–Peppas. Based on the highest correlation coefficients (R^2), the Korsmeyer-Peppas model provided the best fit for both MTX-SLNs and MTX-EDTA-SLNs under physiological conditions (pH 7.4, Fig. 5 and 6; Table 5) as well as acidic conditions (pH 5.5, Fig. 7 and 8; Table 6). Fitting to the Korsmeyer-Peppas framework indicates that MTX release from the lipid matrix is primarily governed by concentration gradient-driven diffusion through the matrix pores.

Table 5: R^2 values of different kinetic models for optimized MTX-SLNs and MTX-EDTA-SLNs for physiological pH 7.4 in PBS

Kinetic models	**R^2 value**	**R^2 value**
Zero order	0.7114	0.6106
First order	0.874	0.8146
Hixson -Crowell model	0.8239	0.7477
k-p model	**0.9931**	**0.9782**
Higuchi model	0.9864	0.9611

The highlighted value indicated the highest value of R^2 for the kinetic models

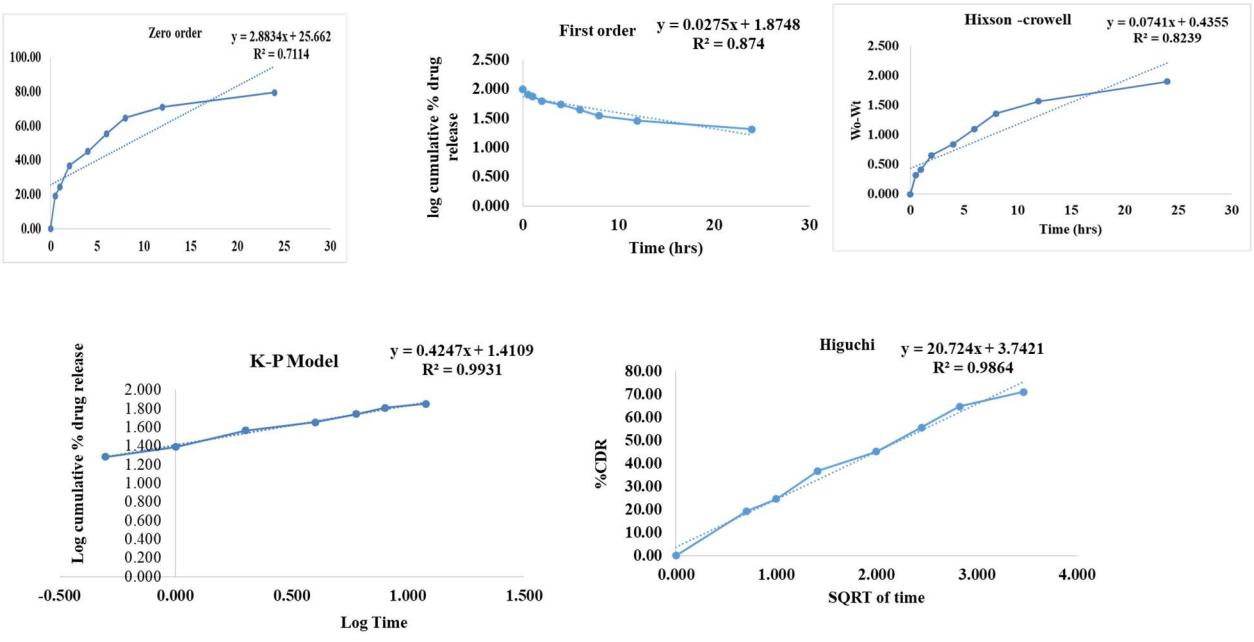

Figure 5: Mathematical models for zero order kinetics (a), first order kinetics (b), hixson-crowell model (c), k-p model (d), and higuchi model (e) for optimized MTX-SLNs for physiological pH 7.4 in PBS

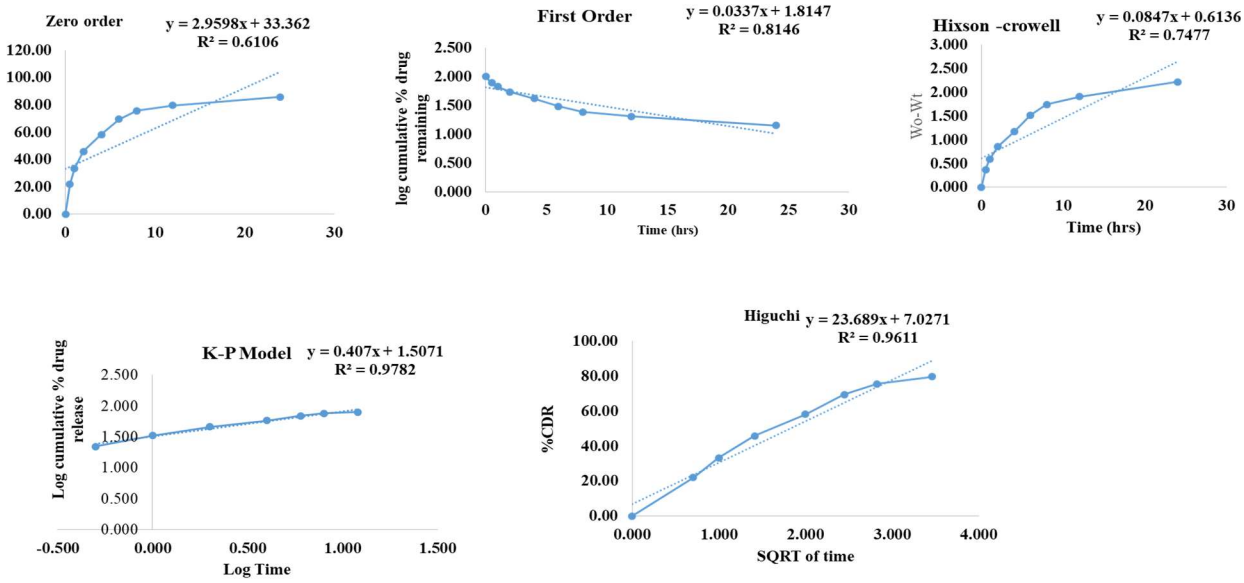

Figure 6: Mathematical models for zero order kinetics (a), first order kinetics (b), hixson-crowell model (c), k-p model (d), and higuchi model (e) for MTX-EDTA-SLNs for physiological pH 7.4 in PBS

Table 6: R^2 values of various kinetic models for optimized MTX-SLNs and MTX-EDTA-SLNs for acidic environment (pH 5.5)

Kinetic models	**R^2 value**	**R^2 value**
Zero order	0 .7351	0.6016
First order	0.9301	0.9101
Hixson -Crowell model	0.8687	0.8160
k-p model	**0.9911**	**0.9884**
Higuchi model	0.9836	0.9669

The highlighted value corresponded to the highest R^2 value for the kinetic models

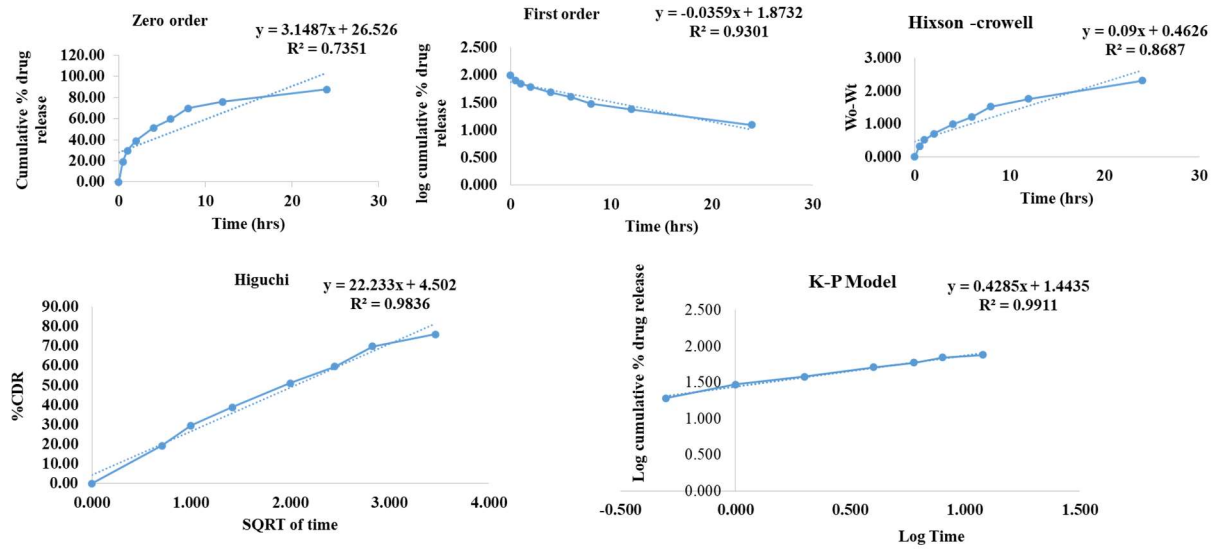

Figure 7: Mathematical models for zero order kinetics (a), first order kinetics (b), hixson-crowell model (c), k-p model (d), and higuchi model (e) for MTX-SLNs for acidic environment pH 5.5

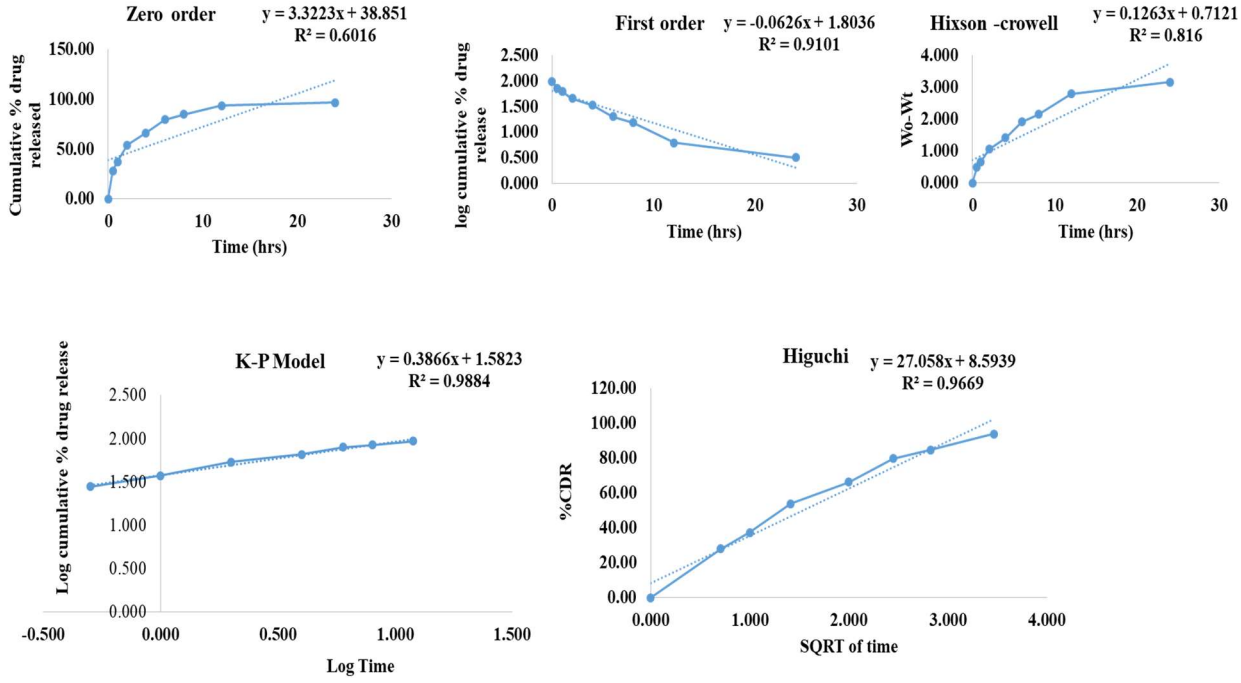

Figure 8: Mathematical models for zero order kinetics (a), first order kinetics (b), hixson-crowell model (c), k-p model (d), and higuchi model (e) for MTX-EDTA-SLNs for acidic environment pH 5.5

7. *In vitro* hemolysis study

To assess the membrane damaging potential of the solid lipid nanoparticles test formulations, a hemolysis assay was performed using erythrocytes. Phosphate buffered saline (PBS, pH 7.4) and 1% Triton X-100 served as the negative and positive controls, respectively. Red blood cells were exposed to the plain drug (MTX), optimized MTX-SLNs and

MTX-EDTA-SLNs (equivalent to 600 µg/mL MTX) and incubated at 37 °C. Erythrocyte lysis was tracked over time (0.5, 2, and 4 h) by centrifuging the samples and reading the supernatant absorbance at 540 nm. The hemolytic profile of free methotrexate (MTX) in comparison to the nanoparticles is illustrated in Figure 9. Initial exposure (0.5 h) revealed that free MTX caused 6.25 ± 4.06% RBC lysis, whereas the optimized MTX-SLNs and MTX-EDTA-SLNs produced significantly lower hemolysis at 1.33 ± 0.27% and 1.23 ± 0.47%, respectively. At 2 h, erythrocyte destruction reached 7.72 ± 3.12% for unformulated MTX, compared to 1.52 ± 0.18% for MTX-SLNs and 1.35 ± 0.45% for MTX-EDTA-SLNs. Over the 4-h, free MTX induced 9.94 ± 3.21% damage, while MTX-SLNs and MTX-EDTA-SLNs maintained minimal values of 1.67 ± 0.19% and 1.44 ± 0.49%, respectively. Overall, free MTX exhibited marked membrane toxicity, whereas both solid lipid nanoparticles formulations produced under 5% hemolysis, classifying them as non-hemolytic per ASTM guidelines [Jhaveri et al., 2018].

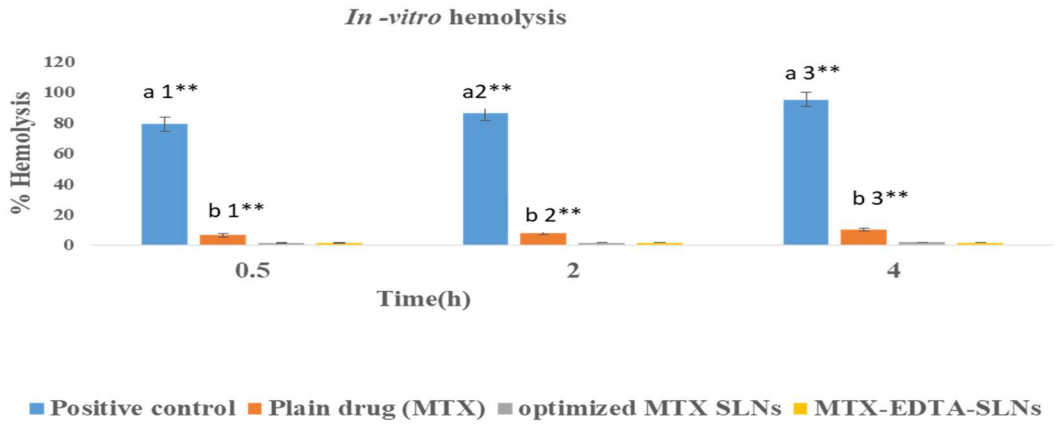

Figure 9: *In vitro* hemolysis of positive control (Triton X100), negative control (normal saline), plain drug (MTX), optimized MTX-SLNs, and MTX-EDTA-SLNs at 0.5, 2, and 4 h intervals, results are shown as mean ± SD (n =3); P < 0.001 indicates statistically highly significant.[a1- Positive control vs plain drug (MTX) and SLNs formulations such as MTX-SLNs and MTX-EDTA-SLNs at time 0.5, a2- Positive control vs plain drug and SLNs formulations at time 2h, a3- Positive control vs Plain drug (MTX) and SLNs formulations at time 4h, b1- plain drug (MTX) vs SLNs formulations at time 0.5, b2- plain drug (MTX) vs SLNs formulations at time 2, b3- plain drug vs SLNs formulations at time 4h

8. Stability studies

Stability testing of the optimized solid lipid nanoparticles formulation was carried out over a three-month period under storage temperatures of 4 ± 1 °C, 25 ± 1 °C, and 40 ± 1 °C in accordance with ICH Q1A(R2) standards for Zone III (Table 7). Crucial quality attributes namely hydrodynamic diameter, zeta potential, and encapsulation efficiency were periodically monitored to ensure physical and chemical stability. When stored at 4 °C, mean particle size exhibited a marginal shift from 123.90 ± 0.43 nm to 125.45 ± 0.49 nm, which was statistically insignificant (ns). At 25 °C, particle size expanded from 123.81 ± 0.35 nm to 127.94 ± 0.25 nm over the study duration, demonstrating statistically significant

variations by month 2 ($p < 0.05$) and month 3 ($p < 0.01$). Storage at 40 °C induced a pronounced size expansion from 123.52 ± 0.27 nm to 131.97 ± 0.51 nm, showing high statistical significance at both month 2 ($p < 0.01$) and month 3 ($p < 0.001$), which points toward thermal induced particle aggregation. Zeta potential remained largely unaltered at 4 °C, shifting non-significantly from −18.70 ± 0.57 mV to −17.96 ± 0.91 mV (ns). Conversely, significant drops in surface charge were detected at 25 °C (from −18.58 ± 0.62 mV to −15.92 ± 0.55 mV; $p < 0.05$ at month 2, $p < 0.01$ at month 3) and at 40 °C (from −18.98 ± 0.80 mV to −14.70 ± 0.41 mV; $p < 0.01$ at month 2, $p < 0.001$ at month 3), reflecting a minor reduction in colloidal stability, though values remained within acceptable limits. Drug entrapment efficiency was preserved at 4 °C (93.45 ± 0.74% to 93.31 ± 0.20%, ns) and displayed only negligible, non-significant decreases at 25 °C and 40 °C. Altogether, the solid lipid nanoparticles formulations maintained optimal physical and chemical stability under refrigerated conditions (4 °C), whereas elevated temperatures accelerated particle growth and surface charge degradation, establishing 4°C as the optimal storage condition.

Table 7: Formulations stability evaluation

Months	Temperature	Particle size	Zeta potential	% Entrapment efficiency
0	4°C± 1°C	123.90 ±0.43	-18.70±0.57	93.45±0.74
	25°C ±1°C	123.81 ±0.35	-18.58±0.62	93.24±0.63
	40°C ±1°C	123.52 ±0.27	-18.98±0.80	93.14±0.50
1	4°C± 1°C	123.94 ±0.29 ^{a1} **ns**	-18.84±0.55 ^{a1} **ns**	93.43±0.90 ^{a1} **ns**
	25°C ±1°C	124.91 ±0.31 ^{b1} **ns**	-17.79±0.35 ^{b1} **ns**	93.11±0.62 ^{b1} **ns**
	40°C ±1°C	124.97 ±0.45 ^{c1} **ns**	-17.97±0.45 ^{c1} **ns**	92.44±0.41 ^{c1} **ns**
2	4°C± 1°C	124.98 ±0.26 ^{a2} **ns**	-17.69±0.91 ^{a2} **ns**	93.35±0.34 ^{a2} **ns**
	25°C ±1°C	126.91 ±0.41 ^{b2*}	-17.46±0.87 ^{b2*}	92.37±0.54 ^{b2} **ns**
	40°C ±1°C	127.94 ±0.25 ^{c2**}	-17.28±0.75 ^{c2**}	92.14±0.64 ^{c2} **ns**
3	4°C± 1°C	**125.45** ±0.49 ^{a3} **ns**	-17.96±0.91 ^{a3} **ns**	93.31±0.20 ^{a3} **ns**
	25°C ±1°C	127.94± 0.25 ^{b3**}	-15.92±0.55 ^{b3**}	93.12± 0.14 ^{b3} **ns**
	40°C ±1°C	131.97± 0.57 ^{c3***}	-14.70±0.41 ^{c3***}	92.10± 0.43 ^{c3} **ns**

Statistical evaluations were carried out using one-way analysis of variance (ANOVA), followed by Tukey's multiple-range post hoc test for pairwise comparisons. Experimental values are reported as mean ± standard deviation (SD) for triplicate measurements (n = 3). Stability over the time was evaluated by comparing post-baseline intervals (months 1, 2, and 3) to the initial time point (month 0) across three distinct thermal conditions: 4 °C (designated by a1, a2, a3), 25°C (designated by b1, b2, b3), and 40°C (coded by c1, c2, c3). Thresholds for statistical significance were established at *p < 0.05, **p < 0.01, and ***p < 0.001, whereas non-significant variations are indicated as "ns".

10. Conclusion

This investigation demonstrates the successful development of a novel dual-agent nanomedicine strategy co-encapsulating methotrexate (MTX) and ethylenediaminetetraacetic acid (EDTA) within solid lipid nanoparticles (SLNs) for targeted breast cancer therapy. The optimized FA-MTX-EDTA-SLNs displayed favorable physicochemical characteristics appropriate for systemic delivery, including less than 200 nm particle size, a low polydispersity index (0.288), negative surface charge, high encapsulation efficiency, and excellent yield (85 ± 0.21%). Drug loading was determined to be 6.2 ± 0.11% for MTX-EDTA-SLNs and 10 ± 0.15% for MTX-SLNs. The stability trials identified 4 ± 1 °C as the optimal storage condition over 3 months. Biocompatibility and hemocompatibility assays confirmed the safety of the solid lipid carriers system. Overall, findings highlight

FA-MTX-EDTA-SLNs as a highly promising platform to overcome therapeutic barriers in breast cancer management, providing a strong rationale for further preclinical in vivo validation.

References

1. Alghnnami, M. H. A., Alamdari, D. H., Haghighi, E., Hosseini, M. M., Khatamian, N., & Tabrizi, M. H. (2025). Evaluate the effects of NLC lipid nanoparticles functionalized with a chitosan-folic acid-methylene blue conjugate on inducing apoptosis in breast cancer cells and inhibiting angiogenesis: An in silico and in vitro investigation. *Results in Chemistry*, 102650.
2. Bhagwat, G. S., Athawale, R. B., Gude, R. P., Md, S., Alhakamy, N. A., Folic acidhmy, U. A., & Kesharwani, P. (2020). Formulation and development of transferrin targeted solid lipid nanoparticles for breast cancer therapy. *Frontiers in pharmacology*, *11*, 614290
3. Cassayre, M., Teles de Souza, D., Claeys-Bruno, M., Altié, A., Piccerelle, P., & Sauzet, C. (2025). Optimization of solid lipid nanoparticle formulation using design of experiments, part I: strategic tool for the determination of critical parameters regarding formulation and process. *Nanomaterials*, *15*(13), 1034.
4. Chaudhari, R., Patel, V., & Kumar, A. (2024). Cutting-edge approaches for targeted drug delivery in breast cancer: beyond conventional therapies. *Nanoscale Advances*, *6*(9), 2270-2286.
5. Chauhan, M., Singh, R. P., Yadav, B., Shekhar, S., Kumar, L., Mehata, A. K., ... & Muthu, M. S. (2023). Dual-targeted transferrin and AS1411 aptamer conjugated micelles for improved therapeutic efficacy and imaging of brain cancer. *Colloids and Surfaces B: Biointerfaces*, *231*, 113544.
6. Chen, Y. H., Tsai, C. Y., Huang, P. Y., Chang, M. Y., Cheng, P. C., Chou, C. H., ... & Wu, C. L. (2007). Methotrexate conjugated to gold nanoparticles inhibits tumor growth in a syngeneic lung tumor model. *Molecular pharmaceutics*, *4*(5), 713-722.
7. da Rocha, M. C. O., da Silva, P. B., Radicchi, M. A., Andrade, B. Y. G., de Oliveira, J. V., Venus, T., ... & Báo, S. N. (2020). Docetaxel-loaded solid lipid nanoparticles prevent tumor growth and lung metastasis of 4T1 murine mammary carcinoma cells. *Journal of nanobiotechnology*, *18*(1), 43.
8. Dadashi, H., Nazemiyeh, A. R., Karimian-Shaddel, A., Mohabbat, A., Folic acidragheh, S. K., Vandghanooni, S., & Eskandani, M. (2024). Enhancing ovarian cancer treatment: Synergistic effects of Methotrexate (Methotrexate)-and quercetin-loaded chitosan nanoparticles. *Carbohydrate Polymer Technologies and Applications*, *8*, 100619.
9. Das, S., Ng, W. K., Kanaujia, P., Kim, S., & Tan, R. B. (2011). Formulation design, preparation and physicochemical characterizations of solid lipid nanoparticles containing a hydrophobic drug: effects of process variables. *Colloids and surfolic acidces b: biointerfolic acidces*, *88*(1), 483-489.
10. De, A., Roychowdhury, P., Bhuyan, N. R., Ko, Y. T., Singh, S. K., Dua, K., & Kuppusamy, G. (2023). Folic acid functionalized diallyl trisulfide–solid lipid nanoparticles for targeting triple negative breast cancer. *Molecules*, *28*(3), 1393.
11. Devi, M., Goswami, P., Koch, B., Kataria, R., Singh, M., Singh, R. P., ... & Jhawat, V. (2026). Folate-targeted, ethylenediaminetetraacetic acid-embedded, methotrexate-loaded albumin nanoparticles: Molecular modeling, design optimization, and in vitro anticancer evaluation in breast cancer cells. *International Journal of Biological Macromolecules*, 152373.
12. Dumoga, S., Dey, N., Kaur, A., Singh, S., Mishra, A. K., & Kakkar, D. (2016). Novel biotin-functionalized lipidic nanocarriers for encapsulating BpT and Bp4eT iron chelators: evaluation of potential anti-tumour efficacy by in vitro, in vivo and pharmacokinetic studies in A549 mice models. *RSC advances*, *6*(66), 61585-61598.
13. Elsayed, A., & Belal, A. (2021). Formulation, characterization and in-vitro evaluation of solid lipid nanoparticles for the delivery of a new anticancer agent, 1H-pyrazolo [3, 4-d] pyrimidine derivative. *Tropical Journal of Pharmaceutical Research*, *20*(5).
14. Garg, N. K., Singh, B., Jain, A., Nirbhavane, P., Sharma, R., Tyagi, R. K., ... & Katare, O. P. (2016). Fucose decorated solid-lipid nanocarriers mediate efficient delivery of Methotrexate in breast cancer therapeutics. *Colloids and Surfolic acidces B: Biointerfolic acidces*, *146*, 114-126.
15. Ghasemiyeh, P., & Mohammadi-Samani, S. (2018). Solid lipid nanoparticles and nanostructured lipid carriers as novel drug delivery systems: applications, advantages and disadvantages. *Research in pharmaceutical sciences*, *13*(4), 288-303.
16. Gidwani, B., & Vyas, A. (2016). Preparation, characterization, and optimization of altretamine-loaded solid lipid nanoparticles using Box-Behnken design and response surfolic acidce

methodology. *Artificial cells, nanomedicine, and biotechnology*, *44*(2), 571-580.

17. Gunduz, U., Keskin, T., Tansık, G., Mutlu, P., Yalcın, S., Unsoy, G., ... & Gunduz, G. (2014). Idarubicin-loaded folic acid conjugated magnetic nanoparticles as a targetable drug delivery system for breast cancer. *Biomedicine & Pharmacotherapy*, *68*(6), 729-736.
18. H. Muller, R., Shegokar, R., & M. Keck, C. (2011). 20 years of lipid nanoparticles (SLN & NLC): present state of development & industrial applications. *Current drug discovery technologies*, *8*(3), 207-227.
19. Hong, W., Guo, F., Yu, N., Ying, S., Lou, B., Wu, J., ... & Yang, G. (2021). A novel folic acid receptor-targeted drug delivery system based on curcumin-loaded β-cyclodextrin nanoparticles for cancer treatment. *Drug design, development and therapy*, 2843-2855.
20. Jhaveri, A., Deshpande, P., Pattni, B., & Torchilin, V. (2018). Transferrin-targeted, resveratrol-loaded liposomes for the treatment of glioblastoma. *Journal of controlled release*, *277*, 89-101.
21. Kakkar, D., Dumoga, S., Kumar, R., Chuttani, K., & Mishra, A. K. (2015). PEGylated solid lipid nanoparticles: design, Methotrexate loading and biological evaluation in animal models. *MedChemComm*, *6*(8), 1452-1463.
22. Kaplan, H. M., & Pazarci, P. (2024). Antiproliferative and apoptotic effects of tempol, Methotrexate, and their combinations on the MCF7 breast cancer cell line. *Acs Omega*, *9*(6), 6658-6662.
23. Khan, Z. A., Tripathi, R., & Mishra, B. (2012). Methotrexate: a detailed review on drug delivery and clinical aspects. *Expert opinion on drug delivery*, *9*(2), 151-169.
24. Lalchandani, D. S., Chenkual, L., Sonpasare, K., Rajdev, B., Naidu, V. G. M., Chella, N., & Porwal, P. K. (2024). Optimization of atorvastatin and quercetin-loaded solid lipid nanoparticles using Box-Behnken design. *Nanomedicine*, *19*(17), 1541-1555.
25. Lu, Y., & Low, P. S. (2002). Folate-mediated delivery of macromolecular anticancer therapeutic agents. *Advanced drug delivery reviews*, *54*(5), 675-693..
26. Mäder, K. (2020). Solid lipid nanoparticles. In *Handbook of Materials for Nanomedicine* (pp. 173-206). Jenny Stanford Publishing.
27. Mohamed, A. A. (2025). Solid Lipid Nanoparticles: Formulation, Evaluation, and Future Prospects. *J. Pharm. Sci*, *5*(4), 23-30.
28. Mukhtar, M., Ezra Manicum, A. L., Shojaei Barjouei, M., Eshaghi Malekshah, R., Behzadmehr, R., Rahdar, A., ... & Baino, F. (2023). Nanocarriers for methotrexate delivery/codelivery in the frame of cancer diagnostics and treatment: a review. *Frontiers in Biomaterials Science*, *2*, 1200670.
29. Niazvand, F., Orazizadeh, M., Khorsandi, L., Abbaspour, M., Mansouri, E., & Khodadadi, A. (2019). Effects of quercetin-loaded nanoparticles on MCF-7 human breast cancer cells. *Medicina*, *55*(4), 114.
30. Priyadarsini, S., & Lahoti, S. R. (2022). Quality by Design: Optimization of Letrozole Solid Lipid Nanoparticle for Breast Cancer. *Indian Journal of Pharmaceutical Education & Research*, *56*(4).
31. Rajpoot, K., & Jain, S. K. (2018). Colorectal cancer-targeted delivery of oxaliplatin via folic acid-grafted solid lipid nanoparticles: preparation, optimization, and in vitro evaluation. *Artificial cells, nanomedicine, and biotechnology*, *46*(6), 1236-1247.
32. Saeg, F., & Anbalagan, M. (2018). Breast cancer stem cells and the challenges of eradication: a review of novel therapies. *Stem cell investigation*, *5*, 39.
33. Sreeharsha, N., Prasanthi, S., Rao, G. S. N. K., Gajula, L. R., Biradar, N., Goudanavar, P., ... & Sreenivasalu, P. K. P. (2025). Formulation optimization of chitosan surfolic acidce coated solid lipid nanoparticles of griseofulvin: A Box-Behnken design and in vivo pharmacokinetic study. *European Journal of Pharmaceutical Sciences*, *204*, 106951.
34. Surve, C. H. A. I. T. A. L. I., Singh, R. U. C. H. I., Banerjee, A. N. A. N. Y. A., Patnaik, S. R. I. N. I. V. A. S., & Shidhaye, S. U. P. R. I. Y. A. (2021). Formulation and qbd based optimization of Methotrexate-loaded solid lipid nanoparticles for an effective anti-cancer treatment. *Int J Appl Pharm*, *13*, 132-43.
35. Suvarsha, G., Velmurugan, R., & Reddy, A. P. (2020). Development and optimization of solid lipid nanoparticle formulation for enhanced solubility of ceritinib using Box–Behnken design. *Asian J Pharm*, *14*(1), 123-32.
36. Thakur, A., Sharma, R., & Devi, A. (2026). Solid lipid nanoparticles for targeted drug delivery in breast cancer: Biointerface interactions, therapeutic potential, and translational challenges. *Pathology-Research and Practice*, 156452.
37. Uzakova, A. B., Yergaliyeva, E. M., Yerlanuly, A., & Mukatayeva, Z. S. (2025). A systematic

review of advanced drug delivery systems: engineering strategies, barrier penetration, and clinical progress (2016–April 2025). *Pharmaceutics*, *18*(1), 11.

38. Yassemi, A., Kashanian, S., & Zhaleh, H. (2020). Folic acid receptor-targeted solid lipid nanoparticles to enhance cytotoxicity of letrozole through induction of caspase-3 dependent-apoptosis for breast cancer treatment. *Pharmaceutical development and technology*, *25*(4), 397-407.
39. Yoon, S. A., Choi, J. R., Kim, J. O., Shin, J. Y., Zhang, X., & Kang, J. H. (2010). Influence of reduced folate carrier and dihydrofolate reductase genes on Methotrexate-induced cytotoxicity. *Cancer research and treatment: official journal of Korean Cancer Association*, *42*(3), 163-171.
40. Zhang, X., Liu, J., Qiao, H., Liu, H., Ni, J., Zhang, W., & Shi, Y. (2010). Formulation optimization of dihydroartemisinin nanostructured lipid carrier using response surface methodology. *Powder Technology*, *197*(1-2), 120-128.